Astron. Astrophys. 318, 768–782 (1997)

ASTRONOMY
AND
ASTROPHYSICS

The spiral galaxy NGC 4559: X-ray point sources and diffuse emission

A. Vogler, W. Pietsch, and F. Bertoldi

Max-Planck-Institut für Extraterrestrische Physik, Giessenbachstraße, D-85740 Garching, Germany

Received 4 November 1995 / Accepted 22 April 1996

Abstract. The inclined nearby (d = 9.7 Mpc) spiral galaxy NGC 4559 was observed with the ROSAT PSPC. Seventeen point sources were detected in a $15' \times 15'$ field, seven of which fall within the D_{25} ellipse of the galaxy. The most luminous source is associated with the nucleus of the galaxy, which has a luminosity of $L_x = 7 \times 10^{39}$ erg s^{-1} and is slightly extended, suggesting a superposition of several compact sources or diffuse emission surrounding a compact central source. The source appears absorbed by a column of $N_{\rm H} = 10^{21}$ cm^{-2}above the Galactic value, so that the intrinsic luminosity of the source exceeds the quoted value by about a factor two. No time variation of the X-ray emission from the central source or any other source in NGC 4559 could be established. The central X-ray source appears slightly offset from the optical center of the galaxy. The larger offset in the soft band may be due to partial shielding through the HI disk of the emission from an extended distribution of X-ray binaries, or diffuse emission surrounding the center.

Another bright source ($L_x = 6 \times 10^{39}$ erg s^{-1}, $N_{\rm H} \simeq 1.7 \times 10^{21}$ cm^{-2}, intrinsic $L_x \gtrsim 1.5 \times 10^{40}$ erg s^{-1}) was found in an outer spiral arm, coincident with an apparent group of HII regions. Since little radio or infrared emission emerges from this location, we conject that the X-rays originate from a single, several 100 year old buried supernova remnant that expands into gas with density of order 10^4 cm^{-3}.

Diffuse, unresolved emission within the galaxy's bulge and inner disk was detected with a total X-ray luminosity of $L_x = 1.5 \times 10^{39}$ erg s^{-1}. Star formation activity at a rate of $\sim 0.2\ M_\odot$ yr^{-1} would produce sufficient X-ray emitting sources to account for this emission. However, the X-rays could also originate from globular cluster X-ray binaries without invoking recent star formation activity.

No emission was detected from a possible halo. In the outer disk we detect a depression of soft X-rays that is likely caused by absorption of soft X-ray background radiation originating beyond the galaxy; the background surface brightness is estimated at $S_x \gtrsim 3 \times 10^{-4}$ cts s^{-1} arcmin^{-2}.

An upper limit of $L_x = 1.9 \times 10^{38}$ erg s^{-1} was derived for the X-ray luminosity of the Type II SN 1941A.

Send offprint requests to: A. Vogler

Key words: galaxies: ISM – galaxies: individual: NGC 4559 – galaxies: spiral – X-rays: galaxies

1. Introduction

X-ray emission from spiral galaxies may arise from compact sources such as active nuclei, accreting binaries, or compact supernova remnants, and from the hot (10^6 K) interstellar medium (HIM) or extended hot gas in a halo, which emits predominantly soft 0.1–0.4 keV X-rays. All these sources are well observable in the ROSAT energy range (0.1–2.4 keV). The good spatial and energy resolution, the high effective area at low energy (0.1–0.4 keV), and the low instrumental background of the ROSAT PSPC for the first time permit to map the diffuse emission and the distribution of faint compact sources in external galaxies.

Since intervening cold gas in the disk of our Galaxy tends to strongly absorb soft X-rays, detailed studies are limited to external galaxies at positions with low galactic foreground absorption. We therefore observed a sample of such spiral galaxies to study their emission components in different environments. We already reported on results for NGC 253 (Pietsch & Trümper 1993), NGC 1566 (Ehle et al. 1996), NGC 4258 (Pietsch et al. 1994), NGC 4449 (Vogler & Pietsch 1996b), NGC 4565, NGC 4656, NGC 5907 (Vogler et al. 1996), and NGC 4631 (Vogler & Pietsch 1996a). All these galaxies contain unresolved, compact sources in their bulges and disks. Galaxies with enhanced star formation or active nuclei also show diffuse emission in the bulge and/or halo, suggestive of hot, tenuous gas and thus consistent with the three component model of the interstellar medium (cf. McKee & Ostriker 1977; Norman & Ikeuchi 1989).

We here present a discussion of the ROSAT PSPC observation of another galaxy in our sample, the highly inclined nearby spiral galaxy NGC 4559 (cf. Table 1), which was not observed during the *Einstein* mission. From these first X-ray images we extracted the point sources and diffuse emission components. We were also able to derive an estimate of the intensity for the diffuse X-ray background.

Table 1. Characteristics of NGC 4559

		Ref.
Type	SABcd	1
Distance	9.7 Mpc ($1' \widehat{=} 2.8$ kpc)	1
Center Position (2000.0)	R.A. $12^h\ 35^m\ 57\overset{s}{.}6$ Dec. $27°57'31''.4$	2
D_{25}	$11'.3$	1
Corrected D_{25}	$9'.6$	1
Axial ratio	0.44	1
Position angle	150°	3
Inclination	69°	1
Galactic foreground N_H	1.5×10^{20} cm^{-2}	4

References:
1 : Tully (1988)
2 : Karachentsev & Kopylov (1990)
3 : SIMBAD data base
4 : Dickey & Lockman (1990)

Table 2. Observation log for NGC 4559

Obs. no.	Date	Obs. intervals	Active time
1	16.06.1993	2	3.1 ks
2	01.07.1994–02.07.1994	5	17.3 ks

2. Observations

NGC 4559 was observed with the ROSAT PSPC (cf. Trümper 1992 for a description of the ROSAT satellite and its detectors) for 20.4 ks during two periods separated by about one year (Table 2). The viewing direction of the satellite was recorded in an "attitude file", and the *Standard Analysis Software System* (SASS, Voges et al. 1992) used to translate the detector coordinates to sky position. This conversion is accurate to $\pm 6''$ (*boresight error*). For both observations a maximum likelihood search for point sources (cf. Sect. 3) was performed, and the X-ray sources were compared with possible optical counterparts, the optical positions of which we obtained from the *Northern Sky Catalogue* finding charts (Irwin et al. 1994). The center position of the first observation had to be corrected by $1''.7$ south, after which both observations were merged. The center position of our ROSAT field is $\alpha = 12^h35^m57\overset{s}{.}3$ and $\delta = 27°57'36''$ (2000.), with a remaining pointing error estimated at $4''$.

3. Data reduction

To permit a sensitive search for diffuse emission, we excluded time intervals with total count rates exceeding 20 cts s^{-1} (average count rate of the observation: 11 cts s^{-1}). The data reduction was performed with the EXSAS software package (Zimmermann et al. 1992). The photon events were binned into 512×512 pixel images, each pixel having a size of $5''$, thus covering a $42'.7$ field of the $2°$ full field of view. The point source detection was performed in each of the five standard energy bands, "broad" (0.11–2.40 keV), "soft" (0.11–0.41 keV), "hard" (0.52–2.01 keV), "hard1" (0.52–0.90 keV), and "hard2" (0.91–2.01 keV). In the inner field of the detector the hard band point spread function (PSF) has a full width at half maximum (FWHM) of $\sim 24''$, the soft band PSF has a FWHM of $\sim 45''$. The detection algorithm and the construction of contour maps are discussed in Vogler & Pietsch (1996a). For a source detection we require a likelihood of existence $L \geqq 10$; the existence probability $P = 1 - e^{-L}$, $L = 10$ corresponds to a Gaussian significance of 3.9σ (cf. Cruddace et al. 1988; Zimmermann et al. 1994a). The count rates were corrected for deadtime, exposure, and vignetting, and two hardness ratios were calculated from the net counts in the subbands as HR1 = (hard–soft)/(hard+soft), and HR2 = (hard2–hard1)/(hard2+hard1). Our contour images were smoothed with the PSF of the individual bands.

4. Results

Fig. 1 shows a contour plot of a smoothed broad-band image for the inner $15' \times 15'$ field of the detector. All identified sources are listed in Table 3 and marked in Fig. 1. Table 3 lists the right ascension and declination (cols. 2 and 3), position errors (col. 4, including a $4''$ systematic error for the attitude solution), likelihood of existence (col. 5), net count with error (col. 6), hardness ratios (cols. 7 and 8) and count rate (col. 9). The likelihood and FWHM of extended sources are listed in column 10.

For a simple conversion of a total measured count rate of a point source or diffuse emission components into an energy flux, we constructed both a 5 keV thermal bremsstrahlung and a 0.4 keV thin thermal plasma spectrum, corrected for Galactic absorption ($N_H = 1.5 \times 10^{20}$ cm^{-2}, cf. Table 1), multiplied by the PSPC response function, and compare the intrinsic energy flux with the simulated ROSAT count rate. The respective conversion factors for the 0.1–2.4 keV ROSAT energy band are listed in Table 4. To estimate errors in the X-ray luminosities due to uncertainties in the choice of spectral model or temperature, we also list the conversion factors for a 0.5 keV thermal bremsstrahlung, and a 4 keV thin thermal plasma spectrum. We find that a variation of temperature by a factor of ten, or the interchange of the models, yields variations in the conversion factors of less than 15%. For point sources at the assumed 9.7 Mpc distance of NGC 4559, from a 5 keV thermal bremsstrahlung spectrum a count rate of 1×10^{-3} cts s^{-1} corresponds to $L_x = 1.5 \times 10^{38}$ erg s^{-1}.

4.1. Sources within the D_{25} ellipse of NGC 4559

Fig. 1 shows seven sources located within the D_{25} ellipse of the galaxy, which represents the optical extent of the galaxy. The two brightest sources, X10, which is located near the optical center, and X7, which is about $2'$ south-west of the nucleus,

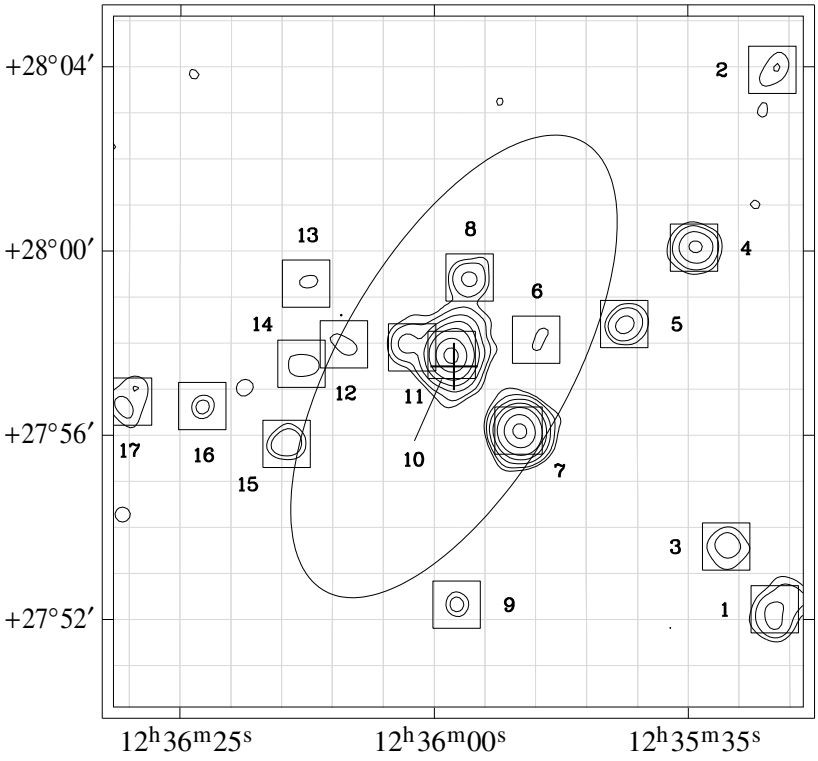

Fig. 1. Contour plot of the broad band ROSAT PSPC image of the inner $15' \times 15'$ of the NGC 4559 field. Contours are 3, 5, 10, 20, 40, 100 and 200 σ above the background ($1\sigma \,\widehat{=}\, 382 \times 10^{-6}$ cts s^{-1} arcmin^{-2}, background $\,\widehat{=}\,$ 1393 $\times$ 10^{-6} cts s^{-1} arcmin^{-2}). ROSAT PSPC detected sources (likelihood $L \geqq 10$) are plotted as squares with ROSAT PSPC source numbers written alongside. The position of the nucleus is marked as a cross. The ellipse outlines the optical extent of the galaxy (D_{25})

yield count rates of $\sim 5 \times 10^{-2}$ cts s^{-1}, corresponding to a luminosity $\sim 7 \times 10^{39}$ erg s^{-1}, corrected only for Galactic, not local absorption. The five next brightest sources yield count rates from 0.9 to 5.2 $\times$ 10^{-3} cts s^{-1} (L_x from 1.4 to 7.9 $\times$ 10^{38} erg s^{-1}). Two of these sources, X8 and X11, are located very near the central emission region, while X6 and X12 are still within the D_{25} ellipse, and only X15 lies on the edge of the stellar disk of NGC 4559.

Fig. 2 shows close-up views of the X-ray emission in the PSPC bands (soft, hard1 and hard2). The soft band shows an arc of diffuse emission protruding from the central region to the east towards X12, which in this band is not identified as a point source because it is well embedded in the extended emission.

Most point sources are detected in the hard bands, and the central source X10 is well separated from the neighboring point sources X11, X8 and X6. We therefore suspect that the diffuse arcs in the soft band are caused by the unresolved superposition of X8/X10/X11 and X12/13/14. The hard2 band shows a wing from the center towards source X6, most likely an additional point source that was not identified by our point source detection algorithm.

4.2. Spectral characteristics of the bright sources X7 and X10

The high photon counts of 849$\pm$30 and 912$\pm$31 for the sources X7 and X10, respectively, permit a detailed spectral analysis. The photons were extracted with a cut radius small enough to avoid contamination from neighboring sources. A proper PSF correction to the extracted regions assured a correct weighting of photons arriving in different energy channels. The data were binned in channels with a signal to noise ratio $\geqq 10$ and simple spectral models were fitted for a thin thermal plasma (TH), a power law (PO), and for thermal bremsstrahlung (BR). Figs. 3 and 4 show the best spectral fits, residuals, and error ellipses for X7 and X10, respectively. Table 5 summarizes the results for the different spectral models; the quoted errors represent 1σ confidence levels.

The central emission region X10 is well fitted by the PO (χ^2/ν = 0.8) and BR (χ^2/ν = 0.7) model, while the TH model fits badly (χ^2/ν = 1.3). Independent of the chosen model, the 0.1–2.4 keV flux, corrected only for Galactic absorption, is 6.5 $\times$ 10^{-12} erg cm^{-2} s^{-1}, corresponding to $L_x \simeq 7.0 \times 10^{39}$ erg s^{-1}. The best spectral fits yield an absorbing column between 8.3 $\times$ 10^{20} cm^{-2} (BR fit) and 10.2 $\times$ 10^{20} cm^{-2} (PO fit) in excess of the Galactic foreground absorption of 1.5 $\times$ 10^{20} cm^{-2}. If the source luminosity is corrected for this absorption, the intrinsic luminosity of X10 is $L_x \simeq 1.2 \times 10^{40}$ erg s^{-1} (0.1 – 2.4 keV) for the bremsstrahlung model.

For X7 the TH model is rejected (χ^2/ν = 11.0), while both the PO and BR models give a good fit to the data. Again the integrated flux, corrected only for Galactic absorption, is nearly independent of the model, and the best fit (PO) yields a luminosity of 6×10^{39} erg s^{-1}. The absorbing column in the direction of X7 is 1.5 $\times$ 10^{21} cm^{-2} in excess of the Galactic foreground for the PO model; for the BR model the excess is 8.7×10^{20} cm^{-2}. If corrected for this additional absorption, the BR model yields an intrinsic $L_x(0.1 - 2.4$ keV) = 1.5 $\times$ 10^{40} erg s^{-1}, and extrapolated, $L_x(0 - 2.4$ keV) = 1.8 $\times$ 10^{40} erg s^{-1}.

Table 3. X-ray properties of point sources within a $15' \times 15'$ field centered on NGC 4559

	R.A. (2000.) (h m s)	Dec. (2000.) (° ′ ″)	R_{err} (″)	Lik.	Net counts	HR1	HR2	Count rate (10^{-3} cts s^{-1})	Extent (Lik., FWHM)
(1)	(2)	(3)	(4)	(5)	(6)	(7)	(8)	(9)	(10)
1	12 35 26.44	+27 52 13.2	9.7	74.6	110.8 ± 13.3	−0.2	−0.3	5.8 ± 0.7	
2	12 35 26.61	+28 03 59.7	16.9	11.3	33.4 ± 9.2	−0.3	−0.9	1.7 ± 0.5	
3	12 35 31.23	+27 53 35.3	12.8	29.4	50.9 ± 9.9	−0.5	0.0	2.6 ± 0.5	
4	12 35 34.37	+28 00 06.8	5.1	115.8	105.2 ± 11.9	0.0	0.0	5.4 ± 0.6	
5	12 35 41.25	+27 58 26.9	6.9	58.4	55.0 ± 9.3	+0.5	+0.4	2.8 ± 0.5	
6	12 35 49.93	+27 58 06.4	14.1	12.9	17.3 ± 4.8	+0.7	+0.7	0.9 ± 0.3	
7	12 35 51.67	+27 56 07.5	1.3	3187.3	848.8 ± 29.9	+0.9	+0.1	43.1 ± 1.5	
8	12 35 56.49	+27 59 28.0	7.1	57.4	54.1 ± 9.2	+0.6	−0.5	2.7 ± 0.5	
9	12 35 57.76	+27 52 19.5	8.8	27.2	23.4 ± 6.5	+1.0	−0.2	1.2 ± 0.3	
10	12 35 58.25	+27 57 46.5	1.5	3194.7	912.1 ± 31.2	+0.9	+0.3	46.2 ± 1.6	35.2, 17.″4
11	12 36 02.14	+27 57 56.5	7.8	55.6	102.7 ± 12.4	+0.2	0.0	5.2 ± 0.6	
12	12 36 08.86	+27 58 00.4	17.2	10.8	25.4 ± 5.9	−0.3	−0.2	1.3 ± 0.3	
13	12 36 12.60	+27 59 19.9	17.2	11.4	30.7 ± 8.5	−0.5	−0.5	1.6 ± 0.4	
14	12 36 13.04	+27 57 34.9	15.0	17.1	34.1 ± 8.8	−0.5	+0.6	1.7 ± 0.4	
15	12 36 14.51	+27 55 49.9	7.2	44.0	46.5 ± 8.6	+0.8	+0.6	2.4 ± 0.4	
16	12 36 22.82	+27 56 39.3	10.3	18.7	28.7 ± 7.4	+1.0	+0.4	1.5 ± 0.4	
17	12 36 30.14	+27 56 45.2	11.8	27.6	49.5 ± 9.6	0.0	+0.1	2.5 ± 0.5	

Table 4. Count rate – energy flux conversion factors for ROSAT PSPC

	BR [1]	BR [1]	TH [2]	TH [2]
Temp.	5 keV	0.5 keV	3 keV	0.3 keV
ECF *	1.36	1.23	1.31	1.19

[1] thermal bremsstrahlung
[2] thin thermal plasma
* in units of 10^{-11} erg cm^{-2} cts^{-1}, corrected for Galactic absorption

Table 5. Spectral parameters of the bright sources X7 and X10

	[1]	N_H (10^{20} cm^{-2})	Index	kT (keV)	χ^2/ν	f_x [2]	L_x [3]
X7	TH	$3.2^{+1.3}_{-0.1}$		$1.5^{+4.4}_{-0.9}$	11.0	4.5	5.0
	BR	$10.0^{+3.8}_{-2.0}$		$0.77^{+0.23}_{-0.14}$	0.8	5.3	5.9
	PO	$16.5^{+10.5}_{-4.0}$	$3.1^{+0.7}_{-0.3}$		0.6	5.6	6.3
X10	TH	$6.0^{+1.3}_{-1.0}$		$4.7^{+4.5}_{-1.7}$	1.3	6.5	7.3
	BR	$9.8^{+4.2}_{-3.3}$		$2.1^{+2.3}_{-0.8}$	0.7	6.4	7.2
	PO	$11.5^{+10.5}_{-3.6}$	$2.0^{+0.6}_{-0.4}$		0.8	6.5	7.3

[1] TH: thin thermal plasma, BR: thermal bremsstrahlung, PO: power law
[2] 0.1–2.4 keV band, corrected for Galactic absorption, in 10^{-13} erg cm^{-2} s^{-1}
[3] flux converted to luminosity, in 10^{39} erg s^{-1}

For both, X7 and X10, the fluxes (corrected for Galactic absorption) obtained via the best fitting spectral model are in good agreement with the values deduced directly from the count rates (Table 3) using the conversion factors of Table 4.

4.3. Radial profiles of the bright sources X7 and X10

To search the bright sources X7 and X10 for extended emission we determined their radial surface brightness profiles to an extraction radius of 50″, and compared these to analytic PSF models. The results are shown in Fig. 5.

Indeed we detected extended emission surrounding the central source X10. Within a ring from 20″ to 50″ we determine an excess count rate of $(6.8 \pm 3.5) \times 10^{-3}$ cts s^{-1} ($L_x = 1.0 \times 10^{39}$ erg s^{-1}). Since our extraction radius is small enough to avoid contributions from X8, X11, or the wing towards the west, the additional emission indicates that X10 is either an extended diffuse source, or a superposition of several point sources. The extended nature of the source is also supported by our point source detection algorithm, which flagged X10 as extended with a FWHM of 17.4″.

For source X7 the analytic PSF model fits the surface brightness well, and no extent was flagged. The difference between the analytic PSF and the measured profile is only $(1.6 \pm 2.3) \times 10^{-3}$ cts s^{-1} in the ring between 20″ and 50″.

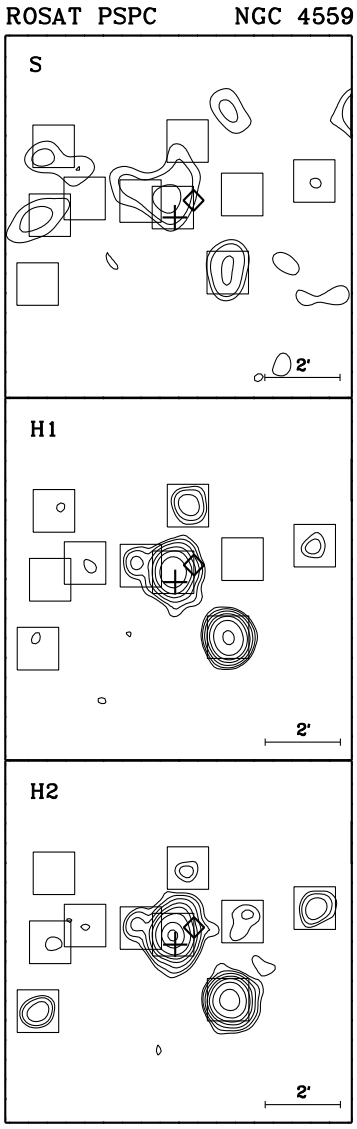

Fig. 2. Contour plots of the central emission region of NGC 4559 for soft (S), hard1 (H1), and hard2 (H2) ROSAT PSPC bands. Soft band contours are given in units of σ (216×10^{-6} cts s^{-1} arcmin^{-2}) above the background (1116×10^{-6} cts s^{-1} arcmin^{-2}), hard band contours (due to the negligible background in these bands) in units of 1.5 photons accumulated per 30″ diameter. One unit = 356×10^{-6} cts s^{-1} arcmin^{-2} for the hard bands. Contour levels are 2, 3, 5, 9, 15, 30, 80 units for all contour plots. The center of NGC 4559 is marked by a cross, detected point sources by squares, the position of SN 1941A north-west of the galaxy's center is marked by a diamond

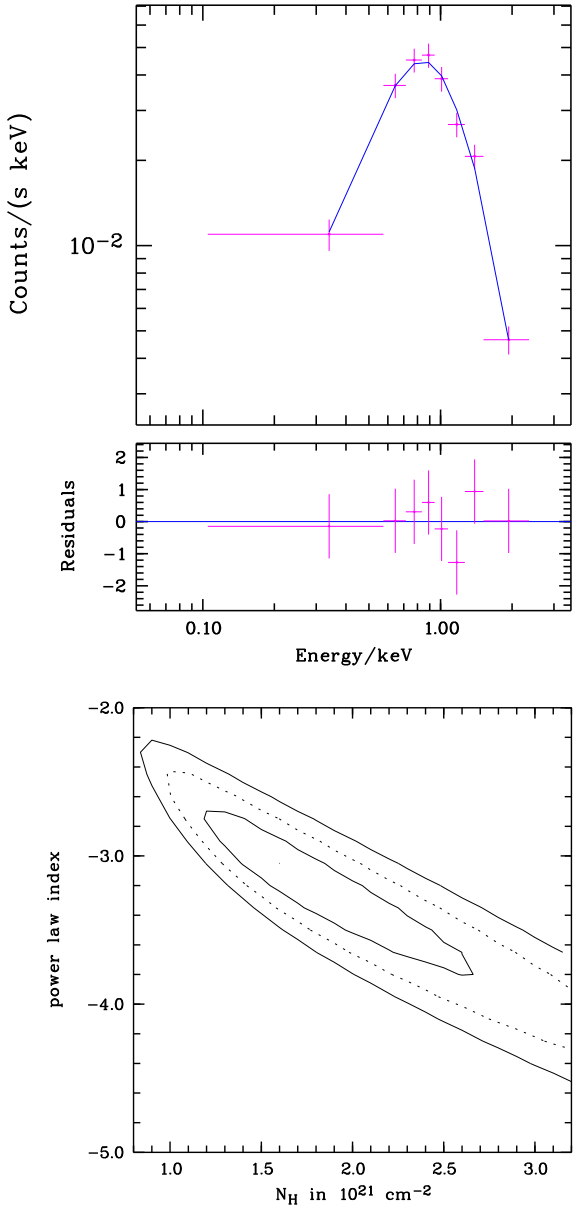

Fig. 3. Results of a power law fit of Source X7: Pulse height spectrum of the total X-ray emission (crosses), best fit spectrum (solid curve, see Table 5 for best fit parameters), and χ^2 contours. The contours correspond to a Gaussian confidence level of 1, 2, and 3σ

4.4. Diffuse emission

We searched for diffuse emission in NGC 4559 within three distinct regions. *Region 1* is defined through a circle with a diameter equal to the minor axis of the D_{25} ellipse, and covers the bulge and inner disk of the galaxy. *Region 2* is defined as the area within the D_{25} ellipse, but outside *region 1*; it contains emission components from the outer disk. Since NGC 4559 is seen under an inclination of 69°, hot halo gas may contribute to both regions. To trace possible halo emission to a greater extent, we defined *region 3* as the area within a circle with a diameter equal to the major axis of the D_{25} ellipse, but outside *regions 1* and *2*. The diffuse emission was studied in the three regions after excluding all identified point sources: X7 and X10 were excluded with cut circles of radius 50″ (cf. Sect. 4.3), all other sources with cut circles of radius R_{90} [1]. The background for the

[1] A circle of radius R_{90} contains 90% of the expected counts for a point source detected by the XRT/detector system in the appropriate energy band and at the respective off-axis angle.

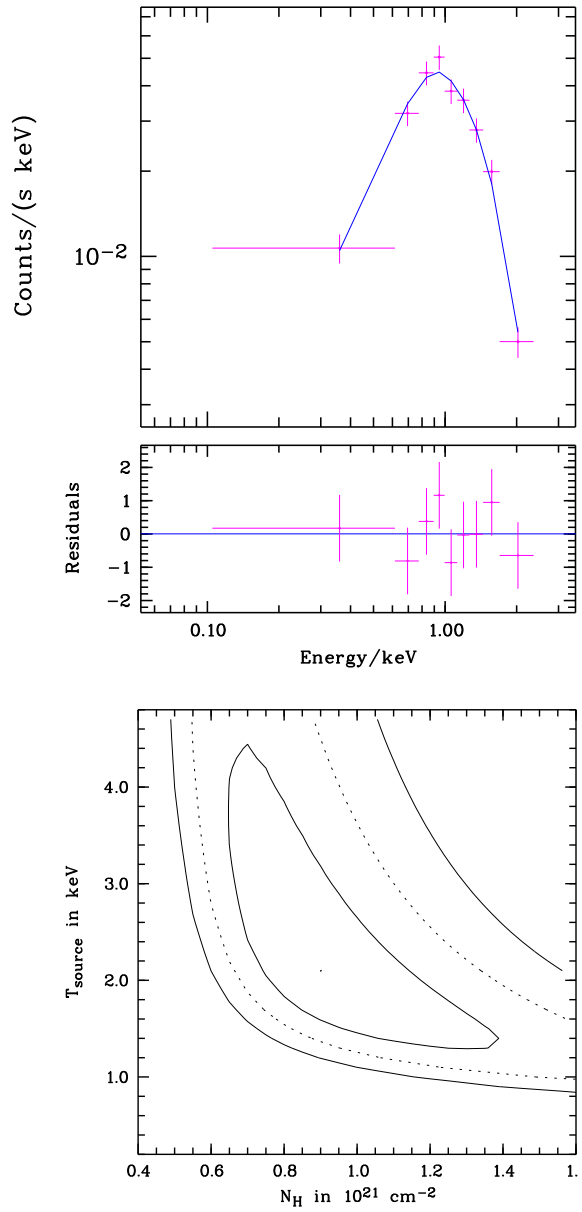

Fig. 4. Results of a thermal bremsstrahlung fit of source X10. See Fig. 3 for explanation

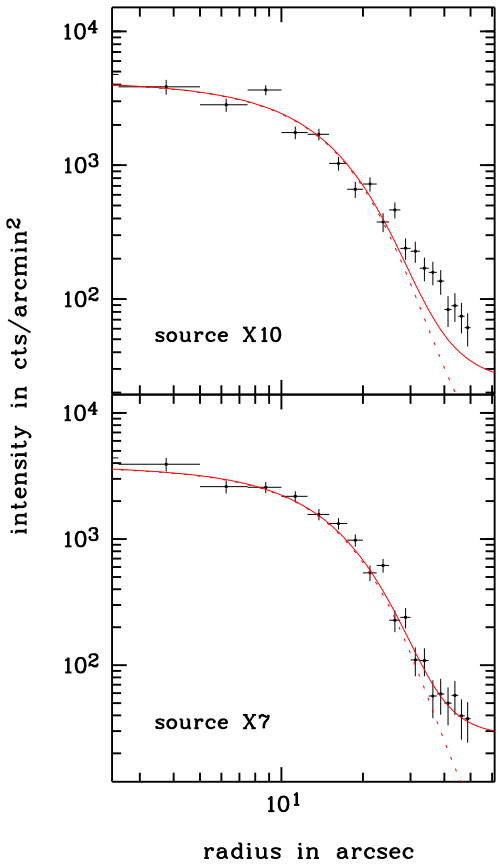

Fig. 5. Radial profiles for source X7 (bottom) and X10 (top) in the ROSAT PSPC 0.1–2.4 keV band. The crosses mark the observed distribution, the curve shows the analytic PSF weighted for the different energy channels. The dotted curves gives the PSF only, the solid one shows the PSF plus the background

energy bands was taken (after excluding point sources) from a $13'$ to $17'$ radius ring.

The total count rates, hardness ratios and luminosities of all point sources and of the diffuse emission in the three regions are listed in Table 6. To determine the luminosities, we assumed a 5 keV thermal bremsstrahlung spectrum for the point sources (cf. Sect. 4), and a thin thermal plasma spectrum with T = 0.3 keV for the diffuse emission. Note that the luminosity for the point sources in the halo (*region 3*) may be in error as some of the sources may be at a distance different from NGC 4559. In order to compare the diffuse emission independent of the extraction area we also calculated the average surface brightnesses, S_x, within each region.

The point sources in *region 1* have an integrated luminosity of $L_x = 1.5 \times 10^{40}$ erg s^{-1}, one order of magnitude higher than the point sources in *region 2*. Diffuse emission from the bulge (*region 1*) is detected with a total luminosity of 4×10^{38} erg s^{-1}. The diffuse emission surrounding the sources X7 and X10 (Sect. 4.3) is not included in this number, and would add another $(7.4 \pm 4.2) \times 10^{-3}$ cts s^{-1}, or $L_x = 1.1 \times 10^{39}$ erg s^{-1}.

For the diffuse emission in the outer disk (*region 2*) we derive a negative count rate of $(-1.3 \pm 1.2) \times 10^{-3}$ cts s^{-1}, which will be discussed in Sect. 5.6. Diffuse emission in *region 3* is not detected at a significant level.

5. Discussion

5.1. Sources within the D_{25} ellipse

We searched the D_{25} ellipse of NGC 4559 (see Table 7) for possible optical, infrared, or radio sources that may be identified with the X-ray point sources. The NASA/IPAC extragalactic database (NED) contains point source catalogues for many different wavelengths (e.g. radio, IRAS, Hα). Optical blue and red plates are available from the PALOMAR II survey, a digitized

Table 6. Emission components of NGC 4559

		Count rate (10^{-3}s^{-1})	HR1	HR2	L_x [1] (10^{39} erg s^{-1})	S_x (10^{37} erg s^{-1}arcmin^{-2})
Region 1	point sources [2]	99.0 ± 3.3	+0.8	+0.2	15.1 ± 0.5	
	diffuse emission [3]	3.0 ± 0.9	+1.0	-1.0	0.4 ± 0.1	3.2 ± 0.9
	diffuse emission [4]	11.4 ± 4.3			1.5 ± 0.6	11 ± 4.1
Region 2	point sources [2]	2.4 ± 0.4	+0.8	+0.6	0.4 ± 0.1	
	diffuse emission	-1.3 ± 1.2				
Region 3	point sources [2]	16.5 ± 1.2	+0.2	+0.2	2.5 ± 0.2	
	diffuse emission	-1.5 ± 1.7				

[1] corrected for Galactic absorption in the 0.1–2.4 keV band, 5 keV thermal bremsstrahlung spectrum for point sources, thin thermal plasma of 0.3 keV for diffuse emission components
[2] point sources in *region 1*: 6, 7, 8, 10, 11, 12; in *region 2*: 15; in *region 3*: 4, 5, 9, 13, 14, 15, 16
[3] excluding X7 and X10, all other point like sources with cut diameters of twice the 90% extraction radius (cf. text)
[4] fitting a PSF to X7 and X10 and excluding all other point sources, with cut diameters of twice the 90% extraction radius (cf. text)

Table 7. Environment of sources within the optical extent (D_{25} ellipse) of NGC 4559

	L_x (10^{38} erg s^{-1})	Environment [1]
X6	1.3 ± 0.5	
X7	63.3 ± 2.2	P: knot on optical plate/HII region ($\Delta \ll 4''$)
X8	4.0 ± 0.7	P: knot on optical plate ($\Delta = 10''$)
		R: coincides with a plateau region of extended radio emission
X10	67.9 ± 2.4	P: center of the galaxy ($\Delta = 15''$),
		R: center of the extended radio emission ($\Delta = 15''$)
X11	7.6 ± 0.9	
X12	1.9 ± 0.5	P: knot on optical plate/HII region ($\Delta \ll 4''$)
		R: point source in radio map ($\Delta = 5''$)
X15	$(3.5 \pm 0.6)^2$	P: faint object ($\Delta = 4''$)

[1] P: Optical plates (J, O, and E); R: 20 cm radio map (Gioia & Fabbiano 1987)
[2] probably not at the distance of NGC 4559 (cf. Sect. 5.1)

plate at 5000 Å from the Digitized Sky Survey DSS (Irwin et al. 1994), and 20 cm radio observations with a beam of $40''$ from Gioia & Fabbiano (1987).

Fig. 6a–e shows the smoothed ROSAT PSPC soft and hard band image contours overlaid onto the 5000 Å plate of NGC 4559. The X-ray source X10 appears slightly offset ($\sim 15''$) from the center of the galaxy, the offset being larger in the soft band ($20''$) than in the hard band ($12''$); in both bands the offsets exceeds the source position error of $4.2''$.

Two sources, X7 and X12, are located in the outer spiral arms of NGC 4559. The J-plate shows knots at these positions, suggesting an identification with HII regions. Source X7 is highly absorbed (cf. Tab. 5) while the hardness ratio HR1= -0.3 for source X12 indicates lower absorption. The low luminosity of X12 ($L_x = 2.0 \times 10^{38}$ erg s^{-1}) does not allow a more detailed spectral investigation.

Source X8 ($L_x = 4.1 \times 10^{38}$ erg s^{-1}) is located near a knot in the inner spiral arms of NGC 4559 ($\Delta = 10''$).

Source X15 is located near the edge of the stellar disk. The *Northern Sky Catalogue* finding charts suggest an identification with a faint background active galactic nucleus (AGN) $4''$ away, so that X15 may not belong to NGC 4559.

At 20 cm NGC 4559 is detected as a radio source that is extended along the optical major axis (Gioia & Fabbiano 1987). The peak of the central X-ray emission and of the radio emission are separated by $15''$, less than the radio beam FWHM of $40''$. Source X7 is located at the edge of the elongated radio structure, and has a total radio flux less than 0.3 mJy. X12 is visible as a point source in the radio map ($5''$ offset). Neither X6 nor X15 show radio counterparts.

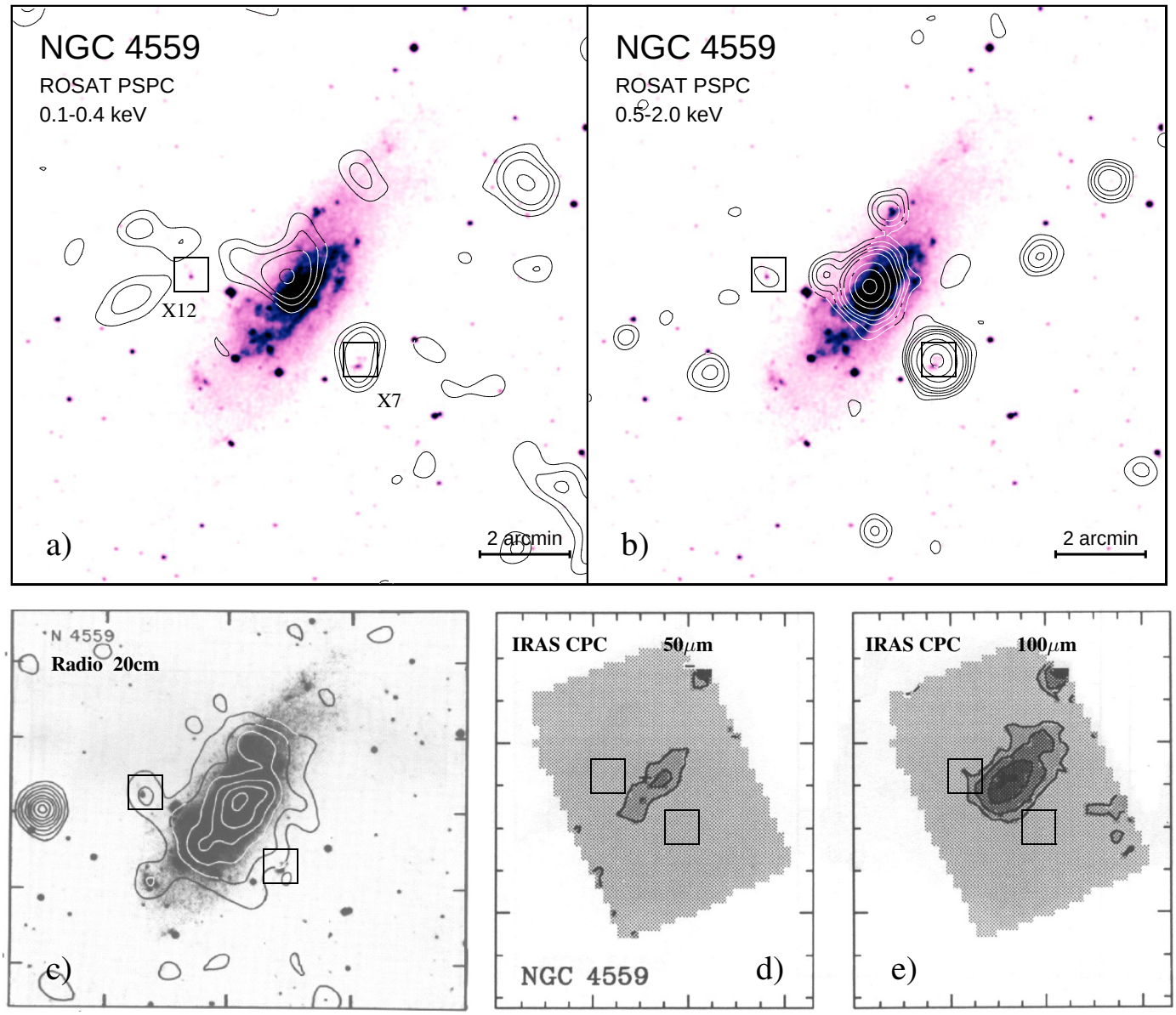

Fig. 6a–e. Observations of NGC 4559 at different wavelengths. **a** and **b** show a short exposed optical image of NGC 4559 (5000 Å plate derived from the digitized sky survey, Irwin et al. 1994) underneath the ROSAT PSPC X-ray contours of the soft and hard band. Contours are 2, 3, 4, 6, 8, 10, and 12σ for the soft band, they are 3, 5, 8, 12, 20, 50, 100 $\times$ 356 $\times$ 10^{-6} cts s^{-1} $arcmin^{-2}$ for the hard band (cf. Fig. 2). **c** gives a 1.5 GHz VLA radio map overlaid onto a blue POSS print (reproduction from Gioia & Fabbiano (1987)); contours are 0.3, 0.9, 1.8, 2.9, 4.1, 5.3, 7.1, 8.9 mJy/beam, beam HPW 39x38". **d** and **e** show IRAS CPC images at 50 μm and 100 μm, respectively (reproduction from van Driel et al. (1993)). The positions of two X-ray sources, X7 (west of the galactic center) and X12 (east), are marked by a square in all figures

Except for the nuclear emission region, none of the X-ray source locations coincide with entries in the NED database or the guide star catalogue.

5.2. Sources outside the D_{25} ellipse of NGC 4559

For sources outside the D_{25} ellipse of NGC 4559 we list possible counterparts suggested by the Northern Sky Catalogue (Irwin et al. 1994) in Table 8; no counterparts were suggested by the NASA/IPAC extragalactic database (NED).

5.3. Extended emission from the X-ray bright central region

The best spectral fit of the central X-ray source X10 suggests a luminosity (from 0.1–2.4 keV, corrected for Galactic absorption only) of $L_x \sim 7.2 \times 10^{39}$ erg s^{-1} and a total absorbing column of 9.8×10^{20} cm^{-2} (cf. Sect 4.2 and Table 5). The strong excess of the measured absorbing column over the galactic foreground $N_{\rm H}$ = 1.5 $\times$ 10^{20} cm^2 is evidence for the extragalactic nature of X10. Huchtmeier & Seiradakis (1985) observed NGC 4559 at 21 cm with the Effelsberg telescope and measured a peak

Table 8. Proposed identifications for PSPC detected sources outside the D_{25} ellipse of NGC 4559. Reference: Northern Sky Catalogue (Irwin et al. 1994)

Source	Identification	B (mag)	R (mag)	B–R (mag)	Δ ($''$)
X3	stellar	21.28	—	<1.28	4
X5	stellar	20.03	19.03	1.00	4
X14	blend	22.24	—	<2.24	5
X15	non-stellar	20.05	19.39	0.66	4
X16	stellar	21.15	—	<1.15	7
X17	stellar	21.90	—	<1.90	5

of $N_{\rm H} \gtrsim 6.6 \times 10^{20}$ cm^{-2}(FWHM $\sim 9'$, assuming 3.64×10^{18}cm^{-2}Jy^{-1}km s^{-1}), clearly showing the presence of neutral H in NGC 4559, although details of its distribution could not be resolved.

The luminosity of X10 exceeds the luminosities typical for a central point source in the bulge of a spiral galaxy without a starburst or AGN, such as NGC 4565 ($L_x = 3 \times 10^{39}$ erg s^{-1}), NGC 4656 ($L_x = 1 \times 10^{38}$ erg s^{-1}), NGC 5907 ($L_x = 3 \times 10^{38}$ erg s^{-1}, cf. Vogler et al. (1996) for the last three galaxies), M 31 ($L_x = 1 \times 10^{39}$ erg s^{-1}, Supper et al. 1996) or M 101 ($L_x = 2 \times 10^{38}$ erg s^{-1}, S. Immler, private communication).

We consider two possibilities regarding the nature of the X10: a superposition of bright point sources located in the bulge of the galaxy, or an AGN. The measured slight extent of X10 (Sect. 4.3) suggests a superposition of several unresolved point sources, possibly with additional extended diffuse emission; a central AGN may still be present. In the absence of an AGN, however, most of the X-ray emission in the central region would be expected to arise from low mass X-ray binaries (LMXBs), many of which are typically located in globular clusters within the bulge of a galaxy. Supper et al. (1996) and Supper (1995), e.g., report such a concentration of LMXBs in the bulge of M 31, where they find 22 point sources with a total luminosity of 1.1×10^{39} erg s^{-1}, plus diffuse, unresolved emission at 4×10^{38} erg s^{-1}.

The emission from X10 could arise from some hundred neutron star binaries radiating close to the Eddington limit of $\sim 3 \times 10^{38}$ erg s^{-1}. For a symmetric distribution of the point sources within the bulge, absorption in the inclined galactic HI disk could account for the observed offset of the soft (0.1–0.4 keV) X-ray emission peak from the optical center. Towards the north-west (the side approaching us), the soft X-ray emission may be shielded by the HI disk, while most hard photons still penetrate the HI layer. However, a uniform HI disk alone could not explain the offset between the 0.5–2.0 keV emission peak and the optical center. This leads us to conject the presence of spatial inhomogeneities in the absorbing gas. While, due to the small optical depth of the soft emission, the soft X-rays are screened more uniformly, hard X-rays are able to leak through holes of less uniform, albeit thicker, HI layers.

From observations at other wavelengths there is no indication that NGC 4559 hosts an active or starburst nucleus (cf. Table 9). A nuclear source was found neither in mid-infrared (MIR) 10 μm, nor in non-thermal radio (NT) observations (Hummel 1980; Gioia & Fabbiano 1987). IRAS observations indicate that the FIR emission peaks at the location of the SN 1941A (R. Assendorp, private communication), which appears to be a site of enhanced star formation. The 2σ upper limit for the MIR luminosity, $L_{\rm MIR} \lesssim 1.5 \times 10^{41}$ erg s^{-1}, is an order of magnitude below values measured for typical Seyferts such as NGC 4258, where $L_{\rm MIR} \sim 2.3 \times 10^{42}$ erg s^{-1} (numerical values from Rieke & Lobofski 1978). Due to high intrinsic absorption the nucleus of the highly inclined galaxy NGC 4258 is not visible as a point source with ROSAT. However, jets ("anomalous spiral arms") thrown out from the nucleus and diffuse emission out of the bulge/halo are detected with $L_x = 2.0 \times 10^{40}$ erg s^{-1} (cf. Pietsch et al. 1994).

In NGC 4565, another spiral galaxy without a known active or starburst nucleus, we found (Vogler et al. 1996) an X-ray bright central emission region with $L_x = 3 \times 10^{39}$ erg s^{-1} (corrected for Galactic absorption), and Rieke & Lobofski found a MIR upper limit (2σ) of $L_{\rm MIR} < 1.7 \times 10^{41}$ erg s^{-1}. Its ratio $L_x/L_{\rm MIR} \gtrsim 5 \times 10^{-2}$ is comparable to that of NGC 4559, where $L_x/L_{\rm MIR} \gtrsim 1 \times 10^{40}/1.5 \times 10^{41} = 7 \times 10^{-2}$.

Hummel (1980) found extended 20 cm radio emission from NGC 4559, but the nucleus was not detected as a point source ($\Gamma_{\rm NT} = 4\pi D^2 F_{\nu,{\rm NT}} \lesssim 7 \times 10^{26}$ erg s^{-1} Hz^{-1}).

A good indicator for the presence of an AGN would be a strong time variation of the X-ray luminosity of X10. We therefore analyzed our data for such variability. To avoid shadowing of targets by the PSPC support structure, the ROSAT satellite 'rocks' with a wobble period of 402 s around the target. We therefore integrated the counts in bins of 402 s (cf. Fig. 7). Assuming a constant X-ray luminosity for the source, we performed a χ^2/ν test and found $\chi^2/\nu = 0.79$. This value translates to a probability of only 23% in favor of a time-dependent source luminosity. This corresponds to a Gaussian significance of 0.4 for a detection of variability above the system level, so that a significant time variability could not be established. The only clear-cut evidence for the presence of an AGN would be the detection of a variable source above 2 keV in the center of the galaxy. This energy range is however not observable with ROSAT.

If X10 did contain an AGN, the AGN may well be surrounded by diffuse X-ray emission. Worrall & Birkinshaw (1996) demonstrated this for several radio galaxies. A possible origin for such diffuse emission may be the presence of X-ray bright jets, such as those detected for the Seyfert II galaxy NGC 4258 (Pietsch et al. 1994; Cecil et al. 1995), or hot gas such as that surrounding the AGN of NGC 1566 (Ehle et al. 1996).

If a jet was present in NGC 4559 and the jet does not lie within the plane of the galaxy, its inclination could – depending on the direction the jet points at – account for the offset between the X-ray and optical peaks in the soft band, since the soft band photons are then absorbed by the HI disk of the galaxy. Further

Table 9. Observations of NGC 4559 at different wavelengths

		L or Γ_{NT} (erg s^{-1} or	Ref. erg s^{-1} Hz^{-1})	SF rate ($M_\odot$ yr^{-1})
nuclear region	MIR (10 μm)	$< 1.5 \times 10^{41}$	1	
	NT (20cm)	$< 7.0 \times 10^{26}$	2	
	X-rays	$> 7.2 \times 10^{39}$		
whole galaxy	FIR (IRAS)	7.3×10^{42}	3	0.2
	NT (20cm)	7.6×10^{27}	4	1.0
	X-rays, point sources	1.5×10^{40}	5	
	X-rays, diffuse	1.3×10^{39}	6	0.24

[1] Rieke & Lebofsky (1978)
[2] Hummel (1980)
[3] Rice et al. (1988)
[4] Gioia & Fabbiano (1987)
[5] this work, X-ray emission from point sources in *region 1* and *region 2*
[6] this work, diffuse X-ray emission out of *region 1*

one might expect strong absorption toward the AGN, which may partly explain the offset measured in the hard band.

If the diffuse emission between a radius of 20″ to 50″ (0.9 kpc to 2.4 kpc) is due to hot gas surrounding the central X-ray bright region, we can estimate the density, mass and cooling time for this gas. Following the model of Nulsen et al. (1984), for a thermally cooling, kT = 0.3 keV (as for NGC 1566) gas in a spherical, uniform cloud in which the gas is clumped with an unknown volume filling factor η, we find for the density, mass, and cooling time of the gas in front of the galactic plane:

$$n_e = 5.5 \times 10^{-3}\ \eta^{-1/2}\ \mathrm{cm}^{-3}\ , \quad (1)$$

$$m = 3.7 \times 10^{6}\ \eta^{1/2}\ M_\odot\ , \quad (2)$$

$$\tau = 1.5 \times 10^{8}\ \eta^{1/2}\ \mathrm{yr}\ . \quad (3)$$

An object rather similar to X10 was detected in the late-type, barred spiral NGC 1313 (Colbert et al. 1995). From its high luminosity (L_x = 6 × 10^{39} erg s^{-1}), compact nature, and the lack of an optical or radio counterpart, Colbert et al. suggest it to be a single massive, accretion-powered object, i.e. an AGN.

5.4. A remarkable source: X7

The absorbing column towards X7 that we estimate from our spectral fits, 1.5×10^{21} cm^{-2} above the Galactic foreground (cf. Table 5), is above the $N_{\rm H} \sim 6 \times 10^{20}$cm^{-2} peak column measured at 21cm towards NGC 4559 (Huchtmeier & Seiradakis 1985). This suggests that X7 is most likely not a galactic foreground star, but is local to NGC 4559, and that much of the absorption may be local to X7.

To quantify the probability of a chance positioning of a foreground or background source similar to X7 within NGC 4559, we counted all sources within a 6×6 deg field surrounding the galaxy that have a count rate comparable or larger than that of X7, 0.04 s^{-1}. We found 20 sources within the 35 deg^2 field, which yields a probability of 7×10^{-3} to find a source of comparable intensity by chance within the D_{25} ellipse of NGC 4559; although the chances are small, they are not negligible.

No radio source has yet been detected at the position of X7. The 20cm VLA map of Gioia & Fabbiano (1987) gives an upper flux limit of 0.3 mJy (cf. Fig. 6c).

We have checked the location of X7 on four available optical images: the PALOMAR II red and blue plates, the DSS ($\sim$ 5000Å) J-Plate (Fig. 6), and an I-band image of $\sim 1'' = 47$pc resolution (M. Dickinson, private communication).[2] X7 is associated with a 25" (1200pc) diameter group of emission knots in a faint outer arm of the galaxy. On the PALOMAR II plates this group divides into four bright knots, two to the north, two south. On the deeper I-band image, about ten more fainter knots appear, most of which merge with the brighter southern or NE sources. All of the brigher sources appear extended at the 1" resolution. The SW knot is brightest on the blue plate, but becomes relatively fainter at shorter wavelengths. The NW knot, which is the faintest of the four bright knots on the blue plate, becomes the brightest of all on the I plate. Although the colors of all other sources are consistent with that of HII regions, the $m_I \simeq$ 19mag red NW knot, both in shape and color appears more like an elliptical background galaxy. With our current ROSAT image we are not able to tell which of the knots is the source of the X-rays. If the NW knot was an elliptical background galaxy, it appears unlikely that it could account for the X-rays, because it would have $L_x/L_B \simeq 10$, three orders of magnitude higher than any known early-type galaxy (cf. Fabbiano 1995). An upcoming HRI observation and optical spectroscopy on the knots should reveal more about the source of the X-rays. Their extended nature, clustering, and location in a spiral arm indicates that the emission knots are HII regions. Such massive star form-

[2] A HST WFPC2 pointing from Dec 30, 1994 towards the center of NGC 4559 unfortunately missed X7.

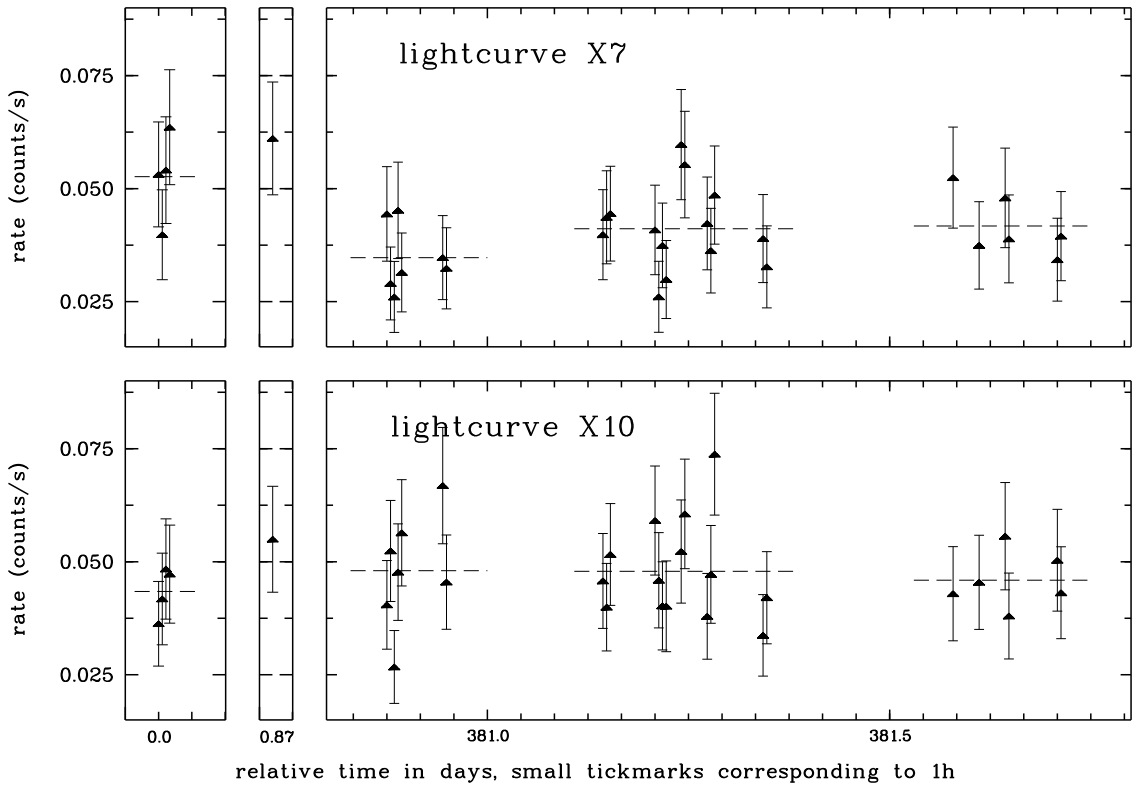

Fig. 7. Lightcurves of X7 (top) and X10 (bottom). The data were binned in intervals corresponding to the 'wobble' period of the satellite (cf. Sect. 5.3). Dashed lines indicate the average count rate for each OBI

ing regions can produce strong X-ray emission from supernovae (SNe) or massive X-ray binaries.

Williams & Chu (1994), e.g., reported X-ray emission from giant HII regions in the nearby galaxy M 101 (NGC 5447, d = 6 Mpc). The brightest HII region in M 101 has a luminosity of 3×10^{38} erg s^{-1} and a temperature $\sim$ 1 keV (assuming $N_{\rm H} = 10^{21}$ cm^{-2} and a thin thermal plasma spectrum). Our spectral analysis of X7 (cf. Sect. 4.2) favors either a power law spectrum with a power law index of 3.1, or a thermal bremsstrahlung spectrum with a temperature of 0.8 keV (9×10^6 K). The best spectral fit for X7 yields a luminosity (0.1-2.4 keV) of $L_x = 6 \times 10^{39}$ erg s^{-1}, uncorrected for the strong intrinsic absorption, or $L_x = 1.5 \times 10^{40}$ erg s^{-1} if corrected for all absorption. Its intrinsic luminosity is thereby *two orders of magnitude higher* than that of the brightest HII region in M 101. In comparison, the typical luminosities of the bright X-ray sources in the LMC (cf. William & Chu 1994 and references therein) are $L_x \lesssim 5 \times 10^{37}$ erg s^{-1} for superbubbles (NGC 44), $L_x \lesssim 5 \times 10^{36}$ erg s^{-1} for SN remnants (N158A), and 2×10^{38} erg s^{-1} for X-ray binaries (LMC X-1).

If the X-rays from X7 indeed arise from a star-forming region (a starburst) with tens of supernova remnants and accreting binaries of typical luminosity, then the large number of massive and possibly young low-mass stars would give rise to a total bolometric luminosity that should exceed the X-ray luminosity by two to three orders of magnitude (Bertoldi & Boller 1996).

Most of the stellar radiation in typical star forming regions is re-radiated by heated dust grains, so that the bolometric luminosity may be estimated from the far infrared (FIR) flux (cf. Rice et al. 1987). Fig. 6a–e shows the IRAS CPC high resolution maps of NGC 4559 (van Driel et al. 1993); neither at 50μm nor at 100μm there appears a source at the marked location of X7. The 3σ detection limit of the observation is 0.6 Jy and 0.5 Jy at 50 and 100μm, respectively. Maximum entropy 12, 25, 60, and 100μm images (R. Assendorp, private communication) also show no emission at X7 (upper limits are 40, 40, 130, and 2000 mJy, whereby at 100μm the detector gets strong emission from the nuclear source at the position of X7), and indicate that the CPC images are misaligned in a way that their peak intensity should coincide with the position of SN 1941A (cf. Fig. 2). For the whole galaxy the IRAS Survey yields $S_\lambda = 0.49, 0.73, 9.69, 27.05$ Jy at $\lambda = 12, 25, 60, 100\mu$m (Rice et al. 1988), whereas the CPC yields S_λ = 7.4 and 44 Jy at 50 and 100μm, respectively. Following the prescription of Rice et al. (1988), at 9.7 Mpc we have

$$L_{\rm FIR} = 1.42 \times 10^{41}\ (2.58[S_{60}/{\rm Jy}] + [S_{100}/{\rm Jy}])\ {\rm erg\ s^{-1}}\ , \quad (4)$$

so that for the whole galaxy, $L_{\rm FIR} = 7.3 \times 10^{42}$ erg s^{-1} (cf. blue luminosity $L_B^0 = 3.7 \times 10^{43}$ erg s^{-1}). The 3σ 100μm CPC detection limit of 0.5 Jy, when scaled to the more reliable IRAS Survey flux, becomes 0.3 Jy. Together with the 60μm limit of 0.13 Jy, we then derive a 3σ detection limit for X7 of $L_{\rm FIR} <$

9×10^{40} erg s^{-1}. Compared with $L_x \simeq 2 \times 10^{40}$ erg s^{-1}, the FIR luminosity appears to be much less than what would be expected from an average star-forming region, which has $L_{\rm FIR}/L_x > 100$. Given a high enough star formation rate, a starburst could produce $L_x = 10^{40}$ erg s^{-1} or more, but would also produce visible and infrared emission with a luminosity two or three orders of magnitude higher than L_x. The high values of $L_x/L_{\rm FIR} > 0.2$ and $L_x/L_B \approx 10$ for X7 cannot arise from a normal star-forming region where X-ray binaries, supernova remnants in a low-density medium, and stars account for the X-rays. The high L_x alone appears very atypical for a star forming region: NGC 4559 contains many other, much brighter giant HII regions that were not detected at all as X-ray sources.

We therefore consider three possibilities concerning the nature of X7, with decreasing likelihood: a single supernova remnant (SNR) expanding into a dense medium, a massive X-ray binary, and an AGN.

5.4.1. Supernova remnant in a dense cloud

Stars form in giant molecular clouds, which are clumpy agglomerates of dense molecular gas. The gas fills only a small fraction of the volume of such a GMC (e.g. Blitz 1991; Bertoldi & McKee 1992) and is eventually ionized and dispersed by the radiation and supernovae of massive stars (Williams & McKee 1995). The possibility that a massive star may explode not only in the tenuous gas of a previously created HII region, but occasionally in the dense molecular gas, has received theoretical interest (Wheeler et al. 1980; Shull 1980) as a possibility to reconcile the discrepant birthrate of pulsars and the observed supernova frequency in the Galaxy (Manchester & Taylor 1977): supernovae in molecular clouds would remain buried, undetectable at optical wavelengths, for a considerable time, and their remnants may cool before they emerge from the obscuring dense gas. The past interest in buried SNRs has faded with the failure to detect any. However, supernovae in high density gas have recently sparked new interest as an alternative explanation concerning the nature of AGN (Terlevich et al. 1992).

The modeling of the evolution and emission spectrum of a buried SNR is subject to large uncertainties arising from the density profile of the molecular cloud, the metallicity of the radiating gas, the abundance and survivability of dust grains, and instabilities in the cooling shocked gas. For an estimate of the parameter ranges that would be consistent with the X-ray and radio luminosity observed for X7 we use the simple expressions of Wheeler et al. (1980) and Shull (1980). Our X-ray observations provide three constraints on the possible ranges of the SNR parameters:

1. The X-ray luminosity, corrected for Galactic and intrinsic absorption, $L_x(0.1-2.4\ {\rm keV}) \simeq 1.6 \times 10^{40}$ erg s^{-1}, is close to the total SNR luminosity.

2. The spectral temperature of (9–18)$\times 10^6$ K derived from the bremsstrahlung and thermal plasma fits are rough estimates of the shocked gas temperature. Below about 3×10^7 K, line cooling should dominate over bremsstrahlung for normal metallicity gas, so that the X-ray spectrum should be dominated by emission lines. However, instabilities in the cooling gas can lead to a wide range of temperatures and the resulting spectrum may not resemble a single temperature model. Terlevich et al. (1992), e.g., point out that for very dense SNRs with high cooling temperatures, the emission spectra in the UV and X-ray range may resemble power laws rather than the exponential drop of a bremsstrahlung spectrum.

3. The intrinsic absorbing column of $\sim 10^{21}$cm^{-2} is comparable to the column of the SNR shell. A larger SNR column would suggest stronger intrinsic absorption and a higher total remnant luminosity. Although this would not affect the spectrum, it seems unreasonable that the remnant has swept up much more mass than that of the surrounding, yet unshocked gas, which must have a column density smaller than the observed.

Consider a supernova ejecta of total initial energy $E = 10^{51}E_{51}$erg expanding into a medium of density $n = 10^4 n_4$ cm^{-3}. A thin shell begins to form when the shocked gas cools on a time scale comparable to the remnant's dynamical time at

$$t_{rad} \simeq 83\ E_{51}^{0.22} n_4^{-0.56}\ {\rm yr}\ , \tag{5}$$

where we assume that line cooling dominates with a cooling function $\Lambda \propto T^{-0.6}$. The temperature of the shocked gas at $t > t_{rad}$ evolves approximately as

$$T_{rad} = 2.7 \times 10^7\ E_{51}^{0.14} n_4^{0.27} (t/t_{rad})^{-10/7}\ {\rm K}, \tag{6}$$

and the total luminosity of the cooling post shock gas is

$$L \simeq 1.0 \times 10^{40}\ E_{51}^{0.78} n_4^{0.56} (t/t_{rad})^{-11/7}\ {\rm erg\ s^{-1}}\ . \tag{7}$$

The column density of the swept-up shell is

$$N_{sh} \simeq 3 \times 10^{21} E_{51}^{0.29} n_4^{0.57} (t/t_{rad})^{2/7} {\rm cm^{-2}}\ . \tag{8}$$

Most of the SN energy is lost between t_{rad} and $3t_{rad}$. In terms of t/t_{rad}, $T_7 = T/10^7$K, and $L_{40} = L/10^{40}$ erg s^{-1} we can solve for the density, SN energy, and shell column:

$$n_4 = (T_7/2.7)^{5.9}\ \ L_{40}^{-1.1}\ \ (t/t_{rad})^{6.8}\ , \tag{9}$$

$$E_{51} = (T_7/2.7)^{-4.2}\ L_{40}^{2.0}\ \ (t/t_{rad})^{-2.9}\ , \tag{10}$$

$$N_{21} = 3(T_7/2.7)^{2.1}\ L_{40}^{-0.014}\ (t/t_{rad})^{3.3}\ . \tag{11}$$

Given $T_7 \simeq 0.9-1.8$ and $L_{40} \simeq 1.6$, we thus find that $n_4 \simeq 1$, $E_{51} \simeq 1$, and $t/t_{rad} \simeq 1-3$ (so that $t \simeq 200$ yr) can reproduce the observed luminosity and temperature of X7 without producing unreasonably high shell column densities. The diameter of the SNR at this point would be of order 0.4 pc or 0.01", well below the resolution of optical telescopes or the VLA; VLBI observations however might be able to reveal the spatial nature of the object.

X7 appears to be a very weak radio emitter. An upper flux limit of 0.3 mJy can be derived from the 1.5 GHz (20 cm) map of Gioia & Fabbiano (1987), which implies a radio luminosity of order $L_R \simeq 10^{35}$ erg s^{-1}. Of the known galactic SNRs, only the Crab Nebula has a comparable value of $L_X/L_R \approx 10^5$; in particular galactic thermal SNR (e.g. Cas-A, Kepler, Tycho) are

weaker in L_X/L_R by factors of 10–100. However, in the galactic remnants, the gas density is significantly lower than that we infer for X7. Since the thermal emissivity scales approximately as n^2 and the synchrotron emission as nB, the luminosity ratio L_X/L_R is expected to rise with increasing density, and the inferred value for X7 is not much out of line from what we might expect from a SNR embedded in a high-density medium. Because of the SNRs high emission measure, EM $> 10^7$pc cm^{-6}, free-free absorption may be able to significantly reduce its radio emission.

Young, X-ray luminous SNRs are not known to be bright sources at visible wavelengths. The SN 1978K in NGC 1313, e.g., is comparable in X-ray luminosity to X7 and shows $L_B/L_x < 0.1$ (Schlegel et al. 1996). Most historical SNRs have visible to X-ray luminosity ratios even below this value. Thus the visible luminosities of the knots coincident with X7 would be consistent with what is expected from a SNR.

Considering the uncertainties in the model assumptions and the strong dependence of n_4 and E_{51} on the age and temperature of the SNR, our estimates can only serve to demonstrate that plausible ranges for the SN energy and gas density could produce a SNR with the observed X-ray properties. We thus conject that X7 is a SNR expanding within a sub-parsec size molecular clump with a density of order 10^4cm^{-3}. The cooling time of the SNR would be several 100 years, long enough that no short-term luminosity variability would be expected. The SNR is associated with a region of moderate star formation activity in a faint outer spiral arm. In such regions there is always a small chance that a higher velocity OB star moves into a dense molecular clump just before it explodes; its short transit time would not leave enough time to clear out the surrounding gas before the explosion.

Colbert et al. (1995) have recently observed the nearby barred spiral galaxy NGC 1313 with the ROSAT PSPC and detected a source very similar to our X7 at the edge of this galaxy's stellar distribution. Their X-2 has a comparable luminosity to that of X7, shows no optical counterpart brigher than $m_V = 21.^m8$, but appears to have decreased by a factor 2 in intensity from its first *Einstein* detection 11 years earlier. Colbert et al. suggest that X-2 is neither a background nor foreground object, but is located in NGC 1313 and may be a compact object powered by accretion, i.e. a black hole candidate. They do not consider the possibility of a buried SNR. Another bright source, X-3 in NGC 1313 is identified with the SN 1978K, which brightened by a factor > 5 from 1980 to 1991 to its current $L_x \simeq 10^{40}$ erg s^{-1} (Ryder et al. 1993; Schlegel et al. 1996). Thus even younger SNRs may become X-ray luminous as their shock encounters high-density circumstellar or interstellar gas.

5.4.2. Black hole accreting binary

If X7 is not a supernova remnant but an accreting, compact neutron star or black hole, as Colbert et al. suggest for their X-2, its observed intrinsic luminosity would require a mass for the accreting object of over 60 $M_\odot$ – assuming it radiates at its Eddington limit for pure electron scattering. The compact star would therefore be a black hole that accretes the ejecta of a low-mass companion. Wind accretion or Roche-lobe overflow from a near-by massive companion appears unlikely because the extreme luminosity of the X-ray source would strongly heat the companion, leading to a very unstable situation. Low-mass X-ray binaries, on the other hand, are observed in our galaxy with much lower luminosities and typically strong variability (cf. Supper et al. (1996) for M31). However, no time variability was observed for X7 (Sect. 5.3), which does not support the accreting binary picture, although it cannot be definitely ruled out.

5.4.3. Galaxy encounter

A more exotic idea for the nature of X7 is an active nucleus of a dwarf galaxy in a close fly-by or merger with NGC 4559. Such an encounter might refuel a dormant AGN, but should leave traces in the structure of NGC 4559. However, there is no indication for tidal disruption or a strong disturbance of its spiral arm patterns. Furthermore, AGN tend to show harder spectra.

5.5. Non-detection of SN 1941A

Within NGC 4559 a Type II supernova explosion was observed in 1941 (SN 1941A, cf. Kowal & Sargent 1971). We do not find excess X-ray emission at its location (marked by a diamond in Fig. 2). The derived 2σ upper limit of 1.3×10^{-3} cts s^{-1} corresponds to $L_x = 2.0 \times 10^{38}$ erg s^{-1} (background taken from a $15''$ to $25''$ radius ring around the position of SN 1941A). Our upper limit is still comparable to the luminosity of a CAS A type supernova remnant in the active galaxy NGC 4449, where ROSAT HRI observations show an X-ray luminous HII region ($L_x = 2.0 \times 10^{38}$ erg s^{-1}) that is apparently heated by the supernova remnant (Vogler & Pietsch 1996b). It is however far below the X-ray luminosities that have been reported from Type II supernovae in NGC 891 (SN 1986J, $L_x > 10^{40}$ erg s^{-1}, Bregman & Pildis 1992), in NGC 1313 (SN 1978K, $L_x > 5 \times 10^{39}$ erg s^{-1}, e.g. Schlegel et al. 1996), and M81 (SN 1993J, $L_x > 10^{39}$ erg s^{-1}, Zimmermann et al. 1994b).

5.6. Diffuse emission

5.6.1. Bulge and inner disk: star formation

In Sect. 4.4 we calculated the diffuse X-ray surface brightness in the innermost *region 1* as 1×10^{38} erg s^{-1} arcmin^{-2}. For comparison, equivalent regions in the edge-on galaxies NGC 4565, NGC 5907, and NGC 4631 show surface brightnesses higher by a factor of two (Vogler et al. 1996; Vogler & Pietsch 1996a). In two of these galaxies, NGC 4565 and NGC 4631, we also detected diffuse emission from a halo. The irregular spiral galaxy NGC 4656, however, shows a surface brightness in *region 1* that is lower by a factor four than that in NGC 4556.

Junkes et al. (1995) propose a model in which the X-ray luminosity due to cooling SN remnants relates to the star formation rate through (cf. Cioffi 1990)

$$L_x \;=\; 5 \times 10^{39} \;\left(\dot{M}_{sf}/M_{\odot}\mathrm{yr}^{-1}\right) \;\; \mathrm{erg\ s}^{-1}\ . \qquad (12)$$

If all of the diffuse emission in *region 1* of NGC 4559 were due to star formation activity, then with a diffuse $L_x \sim 1 \times 10^{39}$erg s^{-1} we derive a star formation rate of 0.25 $M_{\odot}$ yr^{-1}. We can compare this rate with estimates based on luminosities at other wavelength regimes. Bertoldi & Boller (1996) suggest a relation of the far infrared (FIR) luminosity and the SF rate

$$\dot{M}_{sf} \;\simeq\; 9.9 \times 10^{-11}(L_{\mathrm{FIR}}/L_{\odot})\ M_{\odot}\ \mathrm{yr}^{-1}\ , \qquad (13)$$

which with the estimate of $L_{\mathrm{FIR}} \simeq 2 \times 10^9 L_{\odot}$ for NGC 4559 (Rice et al. 1988) yields a SF rate of 0.20 $M_{\odot}$ yr^{-1}, in good agreement with the X-ray estimate.

From the non-thermal radio emission we derive a star formation rate of $\sim 1 M_{\odot}$ yr^{-1} (the radio luminosity of NGC 4559 from Gioia & Fabbiano (1987) is listed in Table 9, the formula for conversion from luminosity to a SF rate in Condon (1992)). This value is higher than the rates deduced from the FIR and X-ray estimates. If the X-rays are absorbed within NGC 4559, the corresponding SF rate may be higher. An initial mass function different from the one assumed may also account for some of the discrepancy; taking an extreme lower mass cut-off of 3.5 $M_{\odot}$ instead of 0.1 $M_{\odot}$ (and a Miller-Scalo IMF), the radio estimate would be lowered by a factor of three.

5.6.2. Outer disk: the X-ray background

In *region 2* we found a negative count rate that exceeds the 1σ error of the measurement. Closer examination reveals that the count rates of the soft and hard bands are (–2.3±1.1) × 10^{-3}cts s^{-1} and (1.2±0.5) × 10^{-3}cts s^{-1}, respectively. A depression exists in the soft band, while we detect unresolved emission in the hard band. The total area, excluding the point sources, over which this flux was measured is 23.8 arcmin^2 for the soft band, so that the negative surface brightness amounts to 1.0×10^{-4} cts s^{-1} arcmin^{-2}.

The HI disk of NGC 4559 has an estimated surface density of $\gtrsim 3 \times 10^{20}$ cm^{-2} in *region 2* (from the map of Huchtmeier & Seiradakis (1985)), so that the transmission of X-ray photons in the 0.1–0.4 keV range is below 10%. This should lead to a strong depression of the X-ray background in the soft band, but not in the hard band, as observed.

A similar effect was found by Snowden et al. (1994) for a region in Ursa Major, by Snowden & Pietsch (1995) in M 101, by Supper (1995) in M 31, and by Warwick (1996) in NGC 55. They estimate the surface brightness of the soft X-ray background as 4.8×10^{-4} cts s^{-1} arcmin^{-2}, $\gtrsim 3.8 \times 10^{-4}$ cts s^{-1} arcmin^{-2}, 7.6×10^{-4} cts s^{-1} arcmin^{-2}, and $\gtrsim 2 \times 10^{-4}$ cts s^{-1} arcmin^{-2}, respectively. Their values were corrected for Galactic HI absorption and assume a power law spectrum with an index of –1.96. For this model we estimate the background brightness at 2.7×10^{-4} cts s^{-1} arcmin^{-2}. The HI map of Huchtmeier & Seradakis (1985) shows that the HI disk of NGC 4559 still measures a column of a few 10^{19} cm^{-2} at a radial distance of 15′ from the galaxy's center. Since we calculated the background in a ring from 13′ to 17′ radius, we must add an additional correction and obtain a background brightness of $\sim 3.4 \times 10^{-4}$ cts s^{-1} arcmin^{-2} with an average surface density of 3×10^{20} cm^{-2}. This value should be perceived as a lower limit for the soft X-ray background since the measured X-ray brightness in *region 2* may still contain residual emission from the galaxy, and because the diffuse X-ray background may not be completely shielded by the HI disk. In any case, our estimate is in quite good agreement with the other measurements.

5.6.3. Region 3

Diffuse emission from *region 3* was not detected at a significant level. The count rate is (-1.5 ± 1.7) cts s^{-1}. The total noise level yields an upper limit to the surface brightness of 4×10^{-5} cts s^{-1} arcmin^{-2}. This is clearly below the measured negative brightness of *region 2* (1×10^{-4} cts s^{-1} arcmin^{-2}). The (2σ) upper limit for the surface brightness of *region 3* is 0.8×10^{37} erg s^{-1} arcmin^{-2}. This upper limit is comparable to upper limits for NGC 4656 (0.6×10^{37} erg s^{-1} arcmin^{-2}) and NGC 5907 (2.6×10^{37} erg s^{-1} arcmin^{-2}), and is clearly below the surface brightness of galaxies for which diffuse emission out of *region 3* was detected, such as NGC 4565 and NGC 4631, which have a surface brightness $\gtrsim 3 \times 10^{37}$ erg s^{-1} arcmin^{-2} (cf. Vogler & Pietsch 1996a; Vogler et al. 1996). However, due to the galactic inclination we cannot rule out that parts of the diffuse emission measured in *region 1* arise from a region above the galactic HI disk and contribute to the halo emission. Nevertheless, the low photon statistics of the diffuse emission did not allow to calculate surface brightness profiles along the major and minor axes to reveal the morphology of the diffuse emission.

6. Summary

We have observed the highly inclined nearby spiral galaxy NGC 4559 with the ROSAT PSPC and detected seventeen point sources in a 15 arcmin field around the galactic center, plus extended unresolved emission from the galaxy and the extragalactic background. Our findings can be summarized as follows:

1. Seven point-like sources were detected within the D_{25} ellipse of the galaxy.
2. No time variation of the X-ray flux from any of the point sources could be detected.
3. The most luminous compact source is slightly extended and almost coincident with the nucleus; its luminosity is 7×10^{39} erg s^{-1}, uncorrected for a shielded by an absorbing column of $N_{\mathrm{H}} \simeq 9 \times 10^{20}$cm^{-2} above the Galactic foreground.
4. The central X-ray source is offset from the optical center of the galaxy. The larger offset in the soft band may be due to partial shielding by the HI disk of emission from either an extended

distribution of X-ray binaries, or diffuse emission surrounding the center.

5. The second bright point source ($L_x = 6 \times 10^{39}$ erg s^{-1} uncorrected, $L_x \gtrsim 1.5 \times 10^{40}$ erg s^{-1} if corrected for its intrinsic shielding column of $N_{\rm H} \simeq 1.7 \times 10^{21}$ cm^{-2}) coincides with a group of HII regions in an outer spiral arm. Little radio or infrared emission emerges from its location. We suggest that the X-rays originate from a single, young supernova remnant that expands into a cloud with density of order 10^4 cm^{-3}.

6. Extended, unresolved emission within the galaxy's bulge and inner disk was detected with a total X-ray luminosity of 1.3×10^{39} erg s^{-1}. Normal star formation at a rate of $\approx 0.2\ M_\odot$ yr^{-1} could account for this emission. However, the X-rays could also originate from globular cluster X-ray binaries without recent star formation.

7. No emission was detected from a possible halo.

8. The soft extragalactic X-ray background is absorbed by the outer disk of NGC 4559, resulting here in a negative net count rate in the soft energy band. From this we estimate the background surface brightness as $S_x \gtrsim 3.2 \times 10^{-4}$ cts s^{-1} arcmin^{-2}, consistent with estimates from other observations.

9. An upper limit of 1.9×10^{38} erg s^{-1} was derived for the X-ray luminosity of the Type II SN 1941A, which could not be detected as a distinct source.

Acknowledgements. We thank our colleagues from the MPE ROSAT group, especially W. Voges, for their support, and R. Assendorp for supplementing the IRAS data. This research has made use of the SIMBAD database operated at CDS, Strasbourg, France and of the NASA/IPAC Extragalactic Database (NED) which is operated by the Jet Propulsion Laboratory, CALTECH, under contract with the National Aeronautics and Space Administration. The ROSAT project is supported by the German Bundesministerium für Bildung, Wissenschaft, Forschung und Technologie (BMBF/DARA) and the Max-Planck-Gesellschaft.

References

Bertoldi F., Boller T., 1996, in prep.
Bertoldi F., McKee C.F., 1992, ApJ 395, 140
Bregman J.N., Pildis R.A., 1994, ApJ 420, 570
Blitz L., 1991, in: Lada C.J., Kylafis N.D. (eds.) The physics of star formation and early stellar evolution, Kluwer, Dordrecht, p. 3
Cecil G., Wilson A.S., dePree C., 1995, ApJ 440, 181
Cioffi D.F., 1990, in: Brinkmann W., Fabian A.C., Giovanelli F. (eds.) Physical Processes in Hot Cosmic Plasmas, NATO ASI series C, 305, p. 1
Colbert E.J.M., Petre R., Schlegel E.M., Ryder S.D., 1995, ApJ 446, 177
Condon J.J., 1992, ARA&A, 30, 575
Cruddace R.G., Hasinger G.R., Schmitt J.H.M.M., 1988, in: Murtagh F., Heck A. (eds.) Astronomy from large databases, ESO Conference and Workshop Proc. 28, p. 177
Dickey J.M., Lockman F.J., 1990, ARA&A 28, 215
van Driel W., de Graauw Th., de Jong T., Wesselius P.R., 1993, A&A 101, 207
Ehle M., Beck R., Haynes R.F., Vogler A., Pietsch W., Elmouttie M., Ryder S., 1996, A&A 306, 73
Gioia I.M., Fabbiano G., 1987, ApJS 63, 771
Huchtmeier W.K., Seiradakis J.H., 1985, A&A 143, 216
Hummel E., 1980, A&AS 41, 151
Irwin M., Maddox S., McMahon R., 1994, Spectrum 2, 14
Junkes N., Zinnecker H., Hensler G., Dahlem M., Pietsch W., 1995, A&A 294, 8
Karachentsev I.D., Kopylov A.I., 1990, MNRAS 243, 390
Kowal C.T., Sargent W.L.W., 1971, AJ 76, 756
Kraus J.D., 1986, Radio Astronomy. Cygnus-Quasar, Powell
Manchester R.N., Taylor J.H., 1977, Pulsars. Freeman, San Francisco
McKee C.F., Ostriker J.P., 1977, ApJ 287, 167
Norman C.A., Ikeuchi S., 1989, ApJ 345, 372
Nulsen P.E.J., Stewart G.C., Fabian A.C., 1984, MNRAS 208, 185
Pietsch W., Trümper J., 1993, Adv. Sp. Res. 13, 171
Pietsch W., Vogler A., Kahabka P., Jain A., Klein U., 1994, A&A 284, 386
Rice W., Lonsdale C.J., Soifer B.T., Neugebauer G., Koplan E.L., Lloyd L.A., de Jong T., Habing H.J., 1988, ApJS 68, 91
Rieke G.H., Lebofsky M.J., 1978, ApJ 220, L37
Ryder S.D., Staveley-Smith L., Dopita M.A., Petre R., Colbert E., Malin D., Schlegel E.M., 1993, ApJ 416, 167
Schlegel E.M., Petre R., Colbert E.J.M., 1996, ApJ 456, 187
Shull J.M., 1980, ApJ 237, 769
Snowden S., Hasinger G., Jahod K., Lockman F. J., McCammon D., Sanders W. T., 1994, ApJ 430, 601
Snowden S.L., Pietsch W., 1995, ApJ 452, 627
Supper R., Hasinger G., Pietsch W., Trümper J., Jain A., Magnier E.A., Lewin W.H.G., van Paradijs J., 1996, A&A, in press
Supper R., 1995, PhD thesis, Ludwig Maximilians Universität, Munich
Terlevich R., Tenorio-Tagle G., Franco J., Melnick J., 1992, MNRAS 255, 713
Trümper J., 1992, QJRAS 33, 165
Tully R.B., 1988, Nearby Galaxies Catalog, Cambridge: Cambridge University Press
Voges W., Gruber R., Paul J., et al., 1992, in: Guyenne T.D., Hunt J.J. (eds.) Proc. European ISY conference, ESA ISY-3, p. 223
Vogler A., Pietsch W., Kahabka P., 1996, A&A 305, 74
Vogler A., Pietsch W., 1996a, A&A 311, 35
Vogler A., Pietsch W., 1996b, A&A, in press
Warwick B., 1996, in: Zimmermann H.U., Trümper J.E., Yorke H. (eds.) Röntgenstrahlung from the universe, MPE Report 263, p. 345
Wheeler J.C., Mazurek T.J, Sivaramakrishnan A., 1980, ApJ 237, 781
Williams R.M., Chu Y.-H., 1994, ApJ 439, 132
Williams J., McKee C.F., 1993, in: The evolution of galaxies and their environment, NASA Ames, p. 167
Worrall D.M., Birkinshaw M., 1996, in: Röntgenstrahlung from the universe, eds. H.U. Zimmermann, J.E. Trümper, H. Yorke, MPE Report 263, p. 531
Zimmermann H.-U., Belloni T., Boese G., et al., 1992, in: Guyenne T.D., Hunt J.J. (eds.) Proc. European ISY conference, ESA ISY-3, p. 231
Zimmermann H.-U. et al., 1994a, EXSAS User Guide, 4th edition, MPE Report 257
Zimmermann H.-U., Lewin W., Predehl P., et al., 1994b, Nat 367, 621

This article was processed by the author using Springer-Verlag LaTeX A&A style file *L-AA* version 3.